IEEE Access
Multidisciplinary ⋮ Rapid Review ⋮ Open Access Journal

Received December 18, 2019, accepted January 26, 2020, date of publication February 5, 2020, date of current version February 14, 2020.

Digital Object Identifier 10.1109/ACCESS.2020.2971708

Three-Dimensional Absolute Attitude Reconstruction of a Rigid Body Based on Multi-Station HRRP Sequences

NAN SU, FENGZHOU DAI, HONGWEI LIU, AND BO ZHANG
Key Laboratory of Radar Signal Processing, Xidian University, Xi'an 710071, China

Corresponding author: Fengzhou Dai (fzdai@xidian.edu.cn)

This work was supported in part by the National Natural Science Foundation of China under Grant 61671359, in part by the Program for the National Science Fund for Distinguished Young Scholars under Grant 61525105, in part by the Shaanxi Innovation Team Project, and in part by the 111 Project under Grant B18039.

ABSTRACT This study proposes a three-dimensional (3-D) absolute attitude reconstruction algorithm of a rigid body target based on multi-station high-resolution range profile (HRRP) sequences. The existing 3-D reconstruction algorithms rely on the target motion form and the reconstructed attitude is inaccurate due to the mismatch of the micro-motion model. In this study, the coordinates of the scattering centers are first calculated from the HRRP sequences of each radar using the factorization method. Then, the multi-station data are associated with the reconstructed scattering center coordinates, and the absolute coordinates is estimated by the relationship between the associated radar line-of-sights (LOSs) and the absolute LOSs. The 3-D reconstruction algorithms for the stable scattering centers and the sliding scattering centers are studied. Numerical simulations verify that the proposed algorithm can reconstruct the 3-D absolute attitude of a rigid body target and is not affected by the mismatch of the target micro-motion model.

INDEX TERMS Absolute attitude, reconstruction before association, factorization method, singular value decomposition (SVD) method.

I. INTRODUCTION

Ballistic missile defense is an important part of a national missile defense system. After the warhead and the missile are separated, there are often many companion targets, including the engine, the debris, and the actively released bait. These companion targets can cause great difficulties for ballistic missile defense, and it is very important to be able to identify the warhead from the numerous false targets and baits in the ballistic missile defense.

After separating from the missile, the warhead performs a spin motion to stabilize the orientation; meanwhile, the lateral force generated during the separation causes a precession upon the warhead: this phenomenon is called micro-motion [1], which is an inherent property of a warhead. Compared with the warhead, the debris and bait do not need to control the attitude and will roll or sway in space. Therefore, the micro-motion characteristics can be used to distinguish a true warhead target from a false one. Many studies have been published on warhead recognition based on target micro-motion characteristics. V. C. Chen proposed that the micro-motion causes a change in the radar echo frequency, called the micro-Doppler frequency [1]. In [2]–[4], different time-frequency analysis methods were proposed to estimate the target micro-motion parameters based on the target narrowband echo. As the radar bandwidth increases, the projection range of the scattering centers can be resolved in the distance dimension. In [5]–[7], the target micro-motion parameters were estimated based on the HRRP sequences or the inverse synthetic aperture radar (ISAR) images. The basis of these algorithms is to build a reasonable micro-motion model of the target. In the micro-motion model, the motion parameters are assumed to be constant. However, the actual target motion is often more complicated. In 3-D space, the warhead is affected by various external forces, causing its motion parameters, such as the precession angle, to change, which leads to the mismatch of the micro-motion model.

The attitude of the target changes with the micro-motion and can be used for warhead identification. Here, the

The associate editor coordinating the review of this manuscript and approving it for publication was Junjie Wu.

absolute attitude of the target is defined as the three-dimensional (3-D) scattering center coordinates of the target in the ground coordinate system. The ISAR image contains the structure and motion information of the target and is widely used in the 3-D absolute attitude reconstruction algorithms [8]–[12]. In [8], the target scattering centers were projected onto the range-Doppler (R-D) plane, and the target image was reconstructed using the projected image sequence. The algorithms in [9]–[11] were based on the interferometric inverse synthetic aperture radar (InISAR). The InISAR system employed multi-radars to obtain multi-view ISAR images, and the height information was obtained using a multi-antenna interference technology. However, the movement of most space targets is complex, as it is characterized by spin, precession, nutation, tumbling, for example, causing the ISAR imaging by standard RD algorithm to be blurred. Thus, some complex algorithms are proposed to solve this problem. In [12], the 3-D coordinates were reconstructed by modeling the equivalent rotational angular velocity by a linear polynomial with time.

With the development of computer vision technology, the 3-D scattering center coordinates reconstruction algorithms based on HRRP sequences were proposed [13]–[19], referring to the 3-D reconstruction algorithm of visual images in the field of computer vision. M. A. Stuff et al. proposed an algorithm to recover the 3-D coordinates of the scattering centers from the 1-D range data using the rigid body invariance property [13]. In [14], a reconstruction algorithm based on the factorization method was proposed, which uses the singular value decomposition (SVD) method to reconstruct the 3-D coordinates of the scattering centers. The reconstruction algorithm based on signal space invariance proposed by [15] is essentially the same as the method in [14]. However, the 3-D attitude reconstruction algorithms in [14] and [15] have ambiguities that cause the solutions of the parameters to not be unique, that is, there is an arbitrary rotation matrix between the reconstructed scattering center coordinates and the real coordinates. Several approaches have been reported to overcome the problem of the rotation ambiguity [16]–[19]. In [16], the 3-D absolute coordinates were extracted by constructing a parameter matrix, which is unique for any rotation translation, but this method degrades as the number of scattering centers and pulses increases. In [17], the relationship between the line-of-sight (LOS) and the target motion parameters was derived, and the arbitrary rotation matrix was calculated based on the relationship; thus, this method fails with the mismatch of the micro-motion model. The same problem exists in [18] and [19], which assumed that the target motion form is known.

Since the absolute attitude of the target is difficult to be reconstructed with the single-station echo, we estimate the absolute scattering center coordinates with the multi-station data. The data association of different radars is the basis of the multi-station 3-D absolute attitude reconstruction. In [20], the distances from the target to the radars were assumed to be much larger than the baseline length between the radars, and the projection positions of the targets on different ISAR images were considered to be substantially the same. In [21], the motion equation of the scattering centers on the R-D image was approximated by a quadratic polynomial, and the Kalman filter (KF) and the nearest-neighbor standard filter (NNSF) were used to associate the scattering centers between different frames. The amplitude of the scattering centers was incorporated to the KF states in [18]. In [22], the speeded up robust features (SURF) were used to extract feature points and estimate the transformation matrix between the ISAR images. The relationship between the rectangular structure on the target and the projection on the ISAR images was deduced with the radar LOS known, and the linear structure on the ISAR images were associated in [23]. These algorithms focus on satellite targets, which contain straight-line structure, and the attitude changes slowly. However, the warhead contains only a few points, and the attitude changes quickly.

In this study, we propose a 3-D absolute attitude reconstruction algorithm based on multi-station HRRP sequences. This algorithm proposes the strategy of ''reconstruction before association''. In the reconstruction step, the single-station 1-D range data are extracted from the echo of each radar and are associated with the KF and the NNSF method. Then, the scattering center coordinates and radar LOS unit vectors are calculated from the 1-D range sequences by the factorization method. In the association step, the multi-station data are associated with the reconstructed scattering center coordinates, and the 3-D absolute attitude of the target is reconstructed by the relationship between the associated LOSs and the absolute LOSs. The 3-D reconstruction algorithms for the stable scattering centers and the sliding scattering centers are studied. Compared with the existing algorithms, the proposed algorithm has the following innovations:

1. There is an arbitrary rotation matrix between the 3-D scattering center coordinates reconstructed by the factorization method and the absolute coordinates. The existing rotation elimination method requires the motion form of the target. The algorithm proposed in this paper draws on the idea of multi-station positioning. After obtaining the relative scattering center coordinates, we reconstruct the absolute scattering center coordinates with the coordinates of multiple radar stations and the target micro-motion model is not required. Thus, the absolute attitude reconstructed by the proposed algorithm is not affected by the mismatch of the micro-motion.

2. Different from the ''association before reconstruction'' strategy adopted in the existing multi-station reconstruction algorithms, the proposed algorithm proposes the strategy of ''reconstruction before association''. Firstly, the 3-D scattering center coordinates of the target are reconstructed with the HRRP sequences of each radar, and then the multi-station data are associated with the reconstructed 3-D coordinates. Compared with the 1-D HRRP or 2-D ISAR image, the 3-D scattering center coordinate contains structural information of the rigid body and is easier to associate.

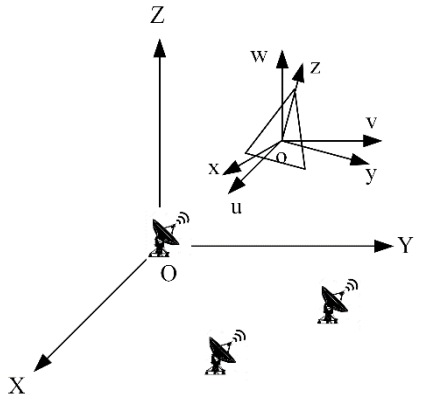

FIGURE 1. Multi-station stable scattering centers reconstruction geometry.

The remainder of the paper is organized as follows: Section II introduces the multi-station 3-D reconstruction geometry and the signal model. Section III presents the single-station scattering center coordinates reconstruction algorithm. Section IV presents the multi-station data association algorithm. Simulation results are given in Section IV, and conclusions are given in Section V.

II. MULTI-STATION 3-D RECONSTRUCTION GEOMETRY AND SIGNAL MODEL

The proper observation geometry and signal model are the basis for further research on 3D reconstruction. In this section, we focus on the multi-station 3-D reconstruction geometry and signal model. According to [30], the spatial target scattering centers can be divided into two types: the first type of scattering centers is fixed on the target body, and does not change with the radar LOS. These scattering centers are called stable scattering centers and include the telemetry window, concavity, and missile tail. The second type of scattering centers, called the sliding scattering centers, appear at the edge of the target and change with the radar LOS. The multi-station reconstruction geometry of the two types of scattering centers and the signal model are given as follows.

A. MULTI-STATION STABLE SCATTERING CENTERS RECONSTRUCTION GEOMETRY

Fig. 1 illustrates the multi-station stable scattering centers reconstruction geometry. To model the problem, the orthogonal coordinate system o-xyz is defined as the object-fixed coordinate system, with the origin being the centroid of the target. O-XYZ is a topocentric coordinate system, whose origin is at a radar in the radar system, referred to as the reference radar, and three coordinate axes point to the east, the north, and the sky direction. Consider a space rigid body target consisting of N scattering centers, whose coordinates in the object-fixed coordinate system is $\mathbf{X}_i = [x_i, y_i, z_i]^{\mathrm{T}}, i = 1, \cdots, N$, and then the ith scattering center coordinate in the topocentric coordinate system at time t_k is given by the following:

$$\tilde{\mathbf{X}}_i(t_k) = \mathbf{R}(t_k)\mathbf{X}_i + \mathbf{T}(t_k) \tag{1}$$

where $\mathbf{R}(t_k)$ and $\mathbf{T}(t_k)$ are the rotation matrix and translation vector between the object-fixed coordinate system and the topocentric coordinate system, respectively. According to [1], the motion of the target can be broken into micro-motion and translation, corresponding to $\mathbf{R}(t_k)$ and $\mathbf{T}(t_k)$, respectively. Here, we assume that the translation of the target is completely compensated and set o-uvw to be the reference coordinate system, whose coordinate axis direction is consistent with that of the topocentric coordinate system, and the origin is at the centroid of the target. The coordinate of the ith scattering center coordinates in the reference coordinate system is given by the following:

$$\bar{\mathbf{X}}_i(t_k) = \mathbf{R}(t_k)\mathbf{X}_i \tag{2}$$

The observation radar network system is composed of M radars, which can meet the synchronization requirements in time and space. The coordinate of the jth radar in the topocentric coordinate system is $\mathbf{Z}_j = \left[z_{xj}, z_{yj}, z_{zj}\right]^{\mathrm{T}}, j = 1, \cdots, M$, and the corresponding radar LOS is $\mathbf{LOS}_j = \left[LOS_{xj}, LOS_{yj}, LOS_{zj}\right]^{\mathrm{T}}, j = 1, \cdots, M$. According to the relationship between the reference coordinate system and the topocentric coordinate system, the jth radar LOS in the reference coordinate system is the same as that in the topocentric coordinate system.

The range of the target is obtained by match filtering. When the bandwidth of the radar is large enough, the scattering centers of the target can be resolved over the radial range. The radial range of the ith scattering center on the jth radar is defined as the inner product of the ith target scattering center coordinate and the jth radar LOS unit vector:

$$\rho_{ij}(t_k) = \bar{\mathbf{X}}_i(t_k)^{\mathrm{T}}\mathbf{LOS}_j \tag{3}$$

where the superscript "T" denotes the transpose. Since the coordinates of the radars can be obtained by the global positioning system (GPS) positioning and the target centroid position can be obtained by the multi-station narrowband positioning [25], the radar LOS unit vectors in the topocentric coordinate system can be calculated. Meanwhile, according to (1), there is only a translation vector $\mathbf{T}(t_k)$ between the reference coordinate system and the topocentric coordinate system, that is, the target centroid position coordinate is also a known parameter. Therefore, the 3-D absolute attitude reconstruction problem studied in this paper is to reconstruct the absolute coordinates of the target scattering centers with the absolute radar LOSs known. For the sake of simplicity, in the following chapters, we refer to the target scattering center coordinates and the unit vectors of the radar LOSs in the reference coordinate system as absolute coordinates and the absolute radar LOS unit vectors, respectively.

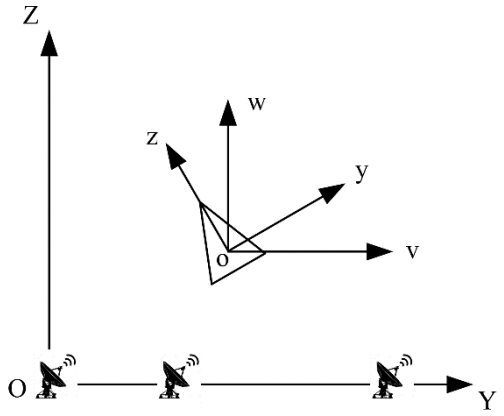

FIGURE 2. Multi-station sliding scattering centers reconstruction geometry.

B. MULTI-STATION SLIDING SCATTERING CENTERS RECONSTRUCTION GEOMETRY

The sliding scattering centers change as the radar LOS changes. Taking a smooth cone as an example, the scattering centers appear at the intersection of the plane formed by the radar LOS and the target symmetry axis with the cone bottom. Since the radar LOS and the sliding scattering centers are always on the same plane, only the change of the radar LOS pitch angle causes the variation of the projection range of the scattering centers, and the azimuth has no effect on the projection distance. Fig. 2 is the multi-station sliding scattering centers reconstruction geometry. The coordinate system in the sliding scattering center reconstruction geometry is similar to that in the stable scattering center reconstruction geometry, except that the radar LOS azimuth is 90° and the coordinate system is two-dimensional. The projection range of the ith sliding scattering center on the LOS of radar j is given by the following:

$$\begin{aligned}\rho_{ij} &= y_i(t_k)\cos(\beta_j) + z_i(t_k)\sin(\beta_j) \\ &= \mathbf{X}_i(t_k)^{\mathrm{T}}\,\mathbf{LOS}_j\end{aligned} \tag{4}$$

where $\mathbf{X}_i(t_k)$ is the coordinate of the ith scattering center in the reference coordinate system at time t_k and β_j is the jth radar LOS pitch angle.

C. SIGNAL MODEL

The carrier frequencies of the radars in the radar network are assumed to be different, which means the signals transmitted by the different radars do not affect each other and the echoes are independent. The jth radar transmits the wideband linear frequency modulation signal can be written as follows:

$$s(\hat{t}, t_k) = \mathrm{rect}\left(\frac{\hat{t}}{T_p}\right)\exp\left(j2\pi\left(f_j t + \frac{1}{2}\mu\hat{t}^2\right)\right) \tag{5}$$

where $\hat{t}$ is the fast time, t is the full time, t_k is the slow time, $t = t_k + \hat{t}$, T_p is the pulse width, f_j is the carrier frequency of the jth radar, μ is the chirp-rate, $\mathrm{rect}(u) = 1$ when $\|u\| \le 0.5$ and $\mathrm{rect}(u) = 0$ when $\|u\| > 0.5$. The transmitted pulse is reflected back after encountering the ith scattering center, and the echo received by the jth radar can be written as follows:

$$\begin{aligned}s_r(\hat{t}, t_k) = A_i\mathrm{rect}&\left(\frac{\hat{t} - \tau_i(t_k)}{T_p}\right) \\ &\cdot \exp\left(j2\pi\left(f_j(t - \tau_i(t_k)) + \frac{1}{2}\mu\left(\hat{t} - \tau_i(t_k)\right)^2\right)\right)\end{aligned} \tag{6}$$

where A_i is the scattering coefficient of the ith scattering center, $\tau_i(t_k) = 2r_i(t_k)/c$, $r_i(t_k)$ is the distance between the ith scattering center and the radar, and c is the speed of light. Since the target translation has been fully compensated, the reference signal is selected as follows:

$$\begin{aligned}s_0(\hat{t}, t_k) = \mathrm{rect}&\left(\frac{\hat{t} - \tau_0}{T_p}\right) \\ &\cdot \exp\left(j2\pi\left(f_j(t - \tau_0) + \frac{1}{2}\mu\left(\hat{t} - \tau_0\right)^2\right)\right)\end{aligned} \tag{7}$$

where $\tau_0 = 2r_0/c$ and r_0 is the distance between the target centroid and the radar. The dechirping procedure is to multiply $s_r(\hat{t}, t_k)$ with the complex conjugate of $s_0(\hat{t}, t_k)$, yielding the following equation:

$$\begin{aligned}s_c(\hat{t}, t_k) = A_i\mathrm{rect}&\left(\frac{\hat{t} - \tau_i(t_k)}{T_p}\right) \\ &\cdot \exp\left(-j2\pi\mu\left(\hat{t} - \tau_0\right)\Delta\tau(t_m)\right) \\ &\cdot \exp\left(-j2\pi f_j\Delta\tau(t_k)\right)\exp\left(j\pi\mu\left(\Delta\tau(t_k)\right)^2\right)\end{aligned} \tag{8}$$

where $\Delta\tau_i(t_k) = \tau_i(t_k) - \tau_0$. The HRRP sequences are obtained by performing a fast Fourier transform operation with the fast time $\hat{t}$ and removing the residual video phase, which results in the following:

$$\begin{aligned}S_c(r, t_k) = A_i\mathrm{sinc}&\left(\frac{2B}{c}(r + \Delta r_i(t_k))\right) \\ &\cdot \exp\left(-j\frac{4\pi}{\lambda}\Delta r_i(t_k)\right)\end{aligned} \tag{9}$$

where $\Delta r_i(t_k) = r_i(t_k) - r_{i0}$. From (7), we can see that the peak of the HRRP modulus $|S_c(r, t_k)|$ appears at $r = -\Delta r_i(t_k)$. Therefore, the peaks of the HRRP can reflect the distance between the target scattering centers to the reference center, that is, the target centroid. To obtain the accurate radial ranges of the scattering centers, we use the iterative adaptive algorithm (IAA) in [26] to obtain the super-resolution result of the HRRP sequences and extract the peak to obtain the 1-D range sequences of the scattering centers. For the details of the algorithm, please refer to reference [26].

III. SINGLE-STATION SCATTERING CENTERS RECONSTRUCTION

Different from the existing algorithm, the proposed algorithm proposes the strategy of ''reconstruction before association''. Firstly, the 3-D scattering center coordinates are reconstructed by the range data of each radar, then,

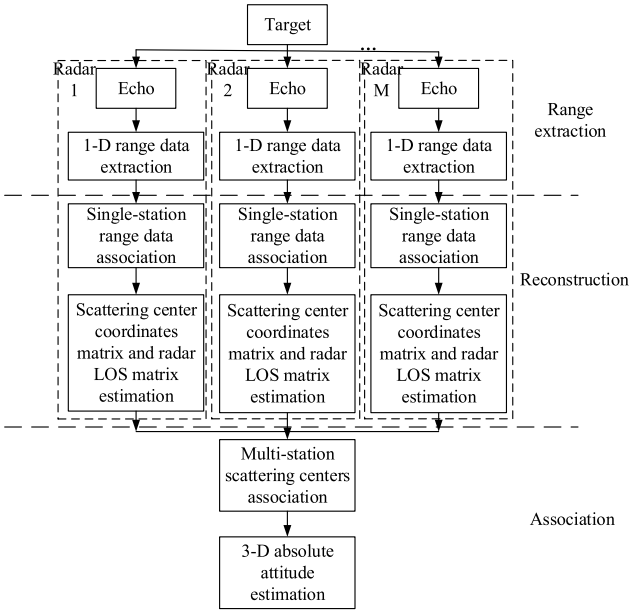

FIGURE 3. Flowchart of the 3-D absolute attitude reconstruction algorithm.

the multi-station data are associated by the reconstructed scattering center coordinates, and the 3-D absolute attitude are reconstructed by the relationship of the associated LOSs and the absolute LOSs. The flowchart of the 3-D absolute attitude reconstruction algorithm based on the multi-station HRRP sequences is shown in Fig. 3. The advantage of this algorithm is that the reconstructed scattering center coordinates contain the structural information of the target and are easy to associate; meanwhile, no prior information of the target motion form is needed. In this section, we introduce the ''reconstruction'' step in the ''reconstruction before association'' strategy.

A. SINGLE-STATION RANGE DATA ASSOCIATION

To reconstruct the 3-D coordinates by using the range data of each radar separately, we need to associate the single-station range data first. The range data association of the scattering centers in the time-range plane is essentially the same as the track association of the point target in the 2-D Cartesian coordinate system in target tracking, thus the track association algorithms such as KF and NNSF [27], Multiple Hypothesis Tracking [18] are used in scattering centers association. Here the KF and NNSF are used to associate the single-station range data considering the issues of simplicity and real-time.

Here, we consider the radial range of the scattering center at each moment as the position of a point target on the time-range plane, and the range sequence as the track of the point target. According to the motion characteristics of the target, the radial range ρ, the velocity v, and the acceleration a of the scattering center do not change much at the adjacent moment, thus we can use constant acceleration model to model the motion, and the KF to associate the radial range of the same scattering center. The state vector of the point target at time t_k is given by the following:

$$\mathbf{g}(k) = \begin{bmatrix} \rho_k & v_k & a_k & t_k & \dot{t}_k & \ddot{t}_k \end{bmatrix}^{\mathrm{T}} \tag{10}$$

where ρ_k and t_k are the position of the point target at time t_k, and v_k, a_k, $\dot{t}$, and $\ddot{t}$ are the velocity and acceleration of the scattering center along the two coordinate axes. The KF is a recursive algorithm that uses the predicted and observed values to estimate the current optimal value, and it contains two steps: the prediction step and the update step. In the prediction step, the target state is predicted with the estimated state in the previous recursive step. In the update step, the target state is updated by a weighted sum of the predicted state and the observation. For the details of the algorithm, please refer to reference [27].

Since the range sequences contain multiple scattering center range data, the problem of the multi-target data association need to be solved. The NNSF is a simple and effective data association algorithm. In the NNSF, first a tracking gate is set, which is centered on the predicted position of the target and the size is guaranteed to correctly receive the echo with a certain probability. Then, the measurement that falls into the tracking gate is regarded as a candidate measurement, that is, the candidate measure meets the following requirement:

$$\left(\mathbf{y}_k - \mathbf{H}\mathbf{g}_{k|k-1}\right)^{\mathrm{T}} \mathbf{S}_k^{-1} \left(\mathbf{y}_k - \mathbf{H}\mathbf{g}_{k|k-1}\right) < \varepsilon \tag{11}$$

where $\mathbf{y}_k$ is the observation, $\mathbf{g}_{k|k-1}$ is the predicted target state, $\mathbf{H}$ is the observation matrix, $\mathbf{S}_k$ is the innovation covariance matrix, which can be obtained in the Kalman prediction step, ε is a small positive value. If only one observation falls into the tracking gate, the coordinates of the observation can be directly used for the Kalman update step. If multiple observations fall into the same tracking gate, the observation with the smallest value in (11) is selected as the candidate observation.

The detailed procedures of the single-station range data association are as follows:

Step 1: Initialize the 1-D range sequences of N scattering centers with the first 5 range data, $k = 5$;

Step 2: Predict the state change of each scattering center using the KF prediction steps.

Step 3: Use the NNSF to select the candidate observations associated with the range sequence of each scattering center;

Step 4: Perform the KF updating steps with the candidate observations, and obtain the updated range data, $k = k + 1$;

Step 5: Repeat Step 2 to Step 4 until $k = K$.

B. 3-D STABLE SCATTERING CENTER RECONSTRUCTION

After the single-station range data association, we obtain the 1-D range sequences of the scattering centers. From (2), we can see that the 1-D radial range sequences are the products of the target scattering center coordinates and the radar LOS unit vectors. According to the coordinate system conversion principle, we can convert the motion of the target into the motion of the radar LOS. Thus, the projection range of the ith scattering center on the radar LOS at time t_k is given

by the following:

$$\rho_{ik} = \mathbf{s}_i^T \mathbf{c}_k \tag{12}$$

where $\mathbf{s}_i$ is the coordinate of the ith scattering center in the object-fixed coordinate system and $\mathbf{c}_k$ is the jth radar LOS unit vector at time t_k in the object-fixed coordinate system. The radial range sequences of the stable scattering centers can be represented as in the matrix-vector form as follows:

$$\mathbf{\Phi}_{N\times K} = \mathbf{S}_{N\times 3}^{\mathrm{T}} \mathbf{C}_{3\times K} \tag{13}$$

where

$$\begin{aligned} \mathbf{\Phi}_{N\times K} &= \begin{bmatrix} \rho_{11} & \rho_{12} & \cdots & \rho_{1K} \\ \rho_{21} & \rho_{22} & \cdots & \rho_{2K} \\ \vdots & \vdots & \ddots & \vdots \\ \rho_{N1} & \rho_{N2} & \cdots & \rho_{NK} \end{bmatrix} \\ \mathbf{S}_{3\times N} &= [\,\mathbf{s}_1 \quad \mathbf{s}_2 \quad \cdots \quad \mathbf{s}_N\,] \\ \mathbf{C}_{3\times K} &= [\,\mathbf{c}_1 \quad \mathbf{c}_2 \quad \cdots \quad \mathbf{c}_K\,] \end{aligned} \tag{14}$$

The 1-D range sequences observation matrix can be represented by

$$\mathbf{Y} = \mathbf{\Phi} + \mathbf{W} \tag{15}$$

where $\mathbf{W}$ is the observation noise matrix.

From (13) we can see that the 1-D range sequences couple the scattering center coordinates and the target motion. When the radar LOS unit vectors can be calculated, the absolute attitude can be evaluated by the relationship between the estimated radar LOSs and the absolute radar LOSs. However, the missiles are usually non-cooperative and the coordinates of the scattering centers are unknown, then the radar LOSs cannot be directly estimated from the 1-D range sequences. According to (15), $\mathbf{S}$ and $\mathbf{C}$ can be obtained by solving the following optimization problem:

$$\begin{aligned} &\min_{\mathbf{S},\mathbf{C}} \left\| \mathbf{Y} - \mathbf{S}^{\mathrm{T}}\mathbf{C} \right\|_2^2 \\ &\text{s.t. } \mathrm{diag}(\mathbf{C}^{\mathrm{T}}\mathbf{C}) = \mathbf{1}_{K\times 1} \end{aligned} \tag{16}$$

where $\mathbf{1}_{K\times 1}$ is a $K \times 1$ identity matrix. The optimization problem can be solved by the factorization method in [17]. The solution steps are as follows:

Step 1 Compute the reduced SVD of observation $\mathbf{Y}$ to obtain $\mathbf{Y}_{N\times K} \approx \mathbf{U}_{N\times 3}\Lambda_{3\times 3}\mathbf{V}_{3\times K}^{\mathrm{T}}$;

Step 2 Form the affine scattering center coordinates matrix $\hat{\mathbf{S}}_A = \mathbf{U}_{3\times N}$ and the affine radar LOS matrix $\hat{\mathbf{C}}_A = \Lambda_{3\times 3}\mathbf{V}_{3\times K}^{T}$;

Step 3 Form a $K \times 6$ matrix $\mathbf{D}$ with the row of the affine radar LOS matrix $\hat{\mathbf{C}}_A$;

Step 4 Calculate the least squares solution of $\mathbf{Dw} = \mathbf{1}_{K\times 1}$ with $M \geq 6$ and obtain the symmetric matrix $\mathbf{W}$;

Step 5 Perform the Cholesky decomposition with $\mathbf{W}$ to obtain the affine transformation matrix $\mathbf{P}$;

Step 6 Form the Euclidean scattering center coordinates matrix $\hat{\mathbf{S}}_E = \mathbf{P}\hat{\mathbf{S}}_A$, and the Euclidean radar LOS matrix $\hat{\mathbf{C}}_E = \mathbf{P}\hat{\mathbf{C}}_A$.

However, there are still infinitely many orthogonal matrices that satisfy the equation:

$$\mathbf{W} = \mathbf{P}^{\mathrm{T}}\mathbf{P} = \mathbf{P}^{\mathrm{T}}\mathbf{O}^{\mathrm{T}}\mathbf{O}\mathbf{P} \tag{17}$$

Thus, a rotation matrix exists between the Euclidean reconstructed coordinates $\hat{\mathbf{S}}_E$ and the absolute coordinates of the scattering centers.

C. 2-D SLIDING SCATTERING CENTER RECONSTRUCTION

Similar to (13), the radial range sequences of the sliding scattering centers have the form

$$\mathbf{\Phi}_{N\times K} = \mathbf{S}_{N\times 2}^{\mathrm{T}} \mathbf{C}_{2\times K} \tag{18}$$

where

$$\begin{aligned} \mathbf{\Phi}_{N\times K} &= \begin{bmatrix} \rho_{11} & \rho_{12} & \cdots & \rho_{1K} \\ \rho_{21} & \rho_{22} & \cdots & \rho_{2K} \\ \vdots & \vdots & \ddots & \vdots \\ \rho_{N1} & \rho_{N2} & \cdots & \rho_{NK} \end{bmatrix} \\ \mathbf{S}_{2\times N} &= [\,\mathbf{s}_1 \quad \mathbf{s}_2 \quad \cdots \quad \mathbf{s}_N\,] \\ \mathbf{C}_{2\times K} &= [\,\mathbf{c}_1 \quad \mathbf{c}_2 \quad \cdots \quad \mathbf{c}_K\,] \end{aligned} \tag{19}$$

$\mathbf{s}_i$ in $\mathbf{S}$ is the coordinates of the ith sliding scattering center in the object-fixed coordinate system, $\mathbf{c}_k$ in $\mathbf{C}$ is the radar LOS unit vector at time t_k. The 2-D Euclidean reconstruction can be obtained by extending the reconstruction algorithm in Section III.B to the 2-D scenario.

IV. MULTI-STATION DATA ASSOCIATION

When the space target is observed by a radar network, the orders of the projection range sequences are not the same due to the different viewing angles of the radars, then the orders of the scattering centers reconstructed by the factorization method are different. Therefore, the multi-station data association is essential for multi-station absolute attitude estimation. In this section we focus on the "association" step in the "reconstruction before association" strategy and estimate the absolute coordinates of the scattering centers.

A. MULTI-STATION SCATTERING CENTERS ASSOCIATION

The essence of multi-station scattering centers association is to find the relationship between the scattering center coordinates reconstructed from the 1-D range data of different radar. According to (17), there exists a rotation matrix between the Euclidean reconstructed coordinates $\hat{\mathbf{S}}_E$ and the absolute scattering centers. Suppose $\mathbf{O}_j$ is the transformation matrix between the scattering center coordinates $\hat{\mathbf{S}}_E^j$ reconstructed from the jth radar and the absolute coordinates $\mathbf{S}_R$, and $\mathbf{O}_j$ is a 3×3 rotation matrix for the stable scattering centers and a 2×2 rotation matrix for the sliding scattering centers, which results in the following:

$$\mathbf{S}_R = \mathbf{O}_j\hat{\mathbf{S}}_E^j \tag{20}$$

The scattering center coordinates reconstructed by the range sequences of the reference radar is set as the reference

coordinates, then the scattering center coordinates reconstructed by the range sequences of the jth radar is given by:

$$\hat{\mathbf{S}}_E^1 = \mathbf{O}_1^{-1}\mathbf{O}_j\hat{\mathbf{S}}_E^j = \mathbf{O}_{j1}\hat{\mathbf{S}}_E^j \tag{21}$$

where $\hat{\mathbf{S}}_E^1$ is the reference coordinates, $\mathbf{O}_1$ is the corresponding rotation matrix, and $\mathbf{O}_{j1}$ is the transformation matrix between $\hat{\mathbf{S}}_E^j$ and $\hat{\mathbf{S}}_E^1$. Since $\mathbf{O}_1$ and $\mathbf{O}_j$ are rotation matrices, $\mathbf{O}_{j1}$ is also a rotation matrix, and $\mathbf{O}_{j1}$ is a 3×3 rotation matrix for the stable scattering centers and a 2×2 rotation matrix for the sliding scattering centers. The scattering centers association problem is transformed into the rotation matrix estimation problem. The transformation error e_i between the ith scattering center coordinate $\hat{\mathbf{s}}_{Ei}^j$ reconstructed from the range sequences of the jth radar and $\hat{\mathbf{s}}_{Ei}^1$ reconstructed from the range sequences of the reference radar is defined as follows:

$$e_i = \left\|\hat{\mathbf{s}}_{Ei}^1 - \mathbf{O}_{j1}\hat{\mathbf{s}}_{Ei}^j\right\|_2 \tag{22}$$

Then the transformation error e between $\hat{\mathbf{S}}_E^j$ and $\hat{\mathbf{S}}_E^1$ can be expressed as the square sum of e_i:

$$e = \sum_{i=1}^{N} e_i^2 = \sum_{i=1}^{N}\left\|\hat{\mathbf{s}}_{Ei}^1 - \mathbf{O}_{j1}\hat{\mathbf{s}}_{Ei}^j\right\|_2^2 \tag{23}$$

The transformation matrix $\mathbf{O}_{j1}$ estimation problem is to find a matrix that minimizes the transformation error e under the condition that the rotation matrix orthogonal constraint is met and can be expressed as follows:

$$\begin{aligned}&\min_{\mathbf{O}_{j1}}\sum_{i=1}^{N}\left\|\hat{\mathbf{s}}_{Ei}^1 - \mathbf{O}_{j1}\hat{\mathbf{s}}_{Ei}^j\right\|_2^2\\ &\text{s.t. } \mathbf{O}_{j1}\mathbf{O}_{j1}^{\mathrm{T}} = \mathbf{O}_{j1}^{\mathrm{T}}\mathbf{O}_{j1} = \mathbf{I}\end{aligned} \tag{24}$$

where $\mathbf{I}$ is a 3×3 identity matrix for the stable scattering centers and a 2×2 identity matrix for the sliding scattering centers. There are two types of methods for solving the above problems: one is the linear algebra method, which is represented by the SVD algorithm [28], and the other is the nonlinear iteration method, which is based on a Lie algebra [29]. Since the nonlinear optimization method has certain requirements on the selection of the initial value selection, and the linear algebra method can obtain the analytical solution, we employ the SVD method proposed in [28] to estimate the rotation matrix $\mathbf{O}_{j1}$.

Expanding the cost function in (23), we have the following:

$$\begin{aligned}&\sum_{i=1}^{N}\left\|\hat{\mathbf{s}}_{Ei}^1 - \mathbf{O}_{j1}\hat{\mathbf{s}}_{Ei}^j\right\|^2\\ &\quad= \sum_{i=1}^{N}\left(\hat{\mathbf{s}}_{Ei}^{1\,T}\hat{\mathbf{s}}_{Ei}^1 - 2\hat{\mathbf{s}}_{Ei}^{1\,\mathrm{T}}\mathbf{O}_{j1}\hat{\mathbf{s}}_{Ei}^j + \hat{\mathbf{s}}_{Ei}^{j^{\mathrm{T}}}\mathbf{O}_{j1}^{\mathrm{T}}\mathbf{O}_{j1}\hat{\mathbf{s}}_{Ei}^j\right)\end{aligned} \tag{25}$$

The first term on the right side of the equation (25) is independent of $\mathbf{O}_j$. The third term is also independent of $\mathbf{O}_j$ due to $\mathbf{O}_{j1}^T\mathbf{O}_j = \mathbf{I}$, and thus the cost function can be rewritten as

$$\begin{aligned}-\sum_{i=1}^{N}\hat{\mathbf{s}}_{Ei}^{1\,T}\mathbf{O}_{j1}\hat{\mathbf{s}}_{Ei}^j &= -\sum_{i=1}^{N}\mathrm{tr}\left(\mathbf{O}_{j1}\hat{\mathbf{s}}_{Ei}^j\hat{\mathbf{s}}_{Ei}^{1\,\mathrm{T}}\right)\\ &= -\mathrm{tr}\left(\mathbf{O}_{j1}\sum_{i=1}^{N}\hat{\mathbf{s}}_{Ei}^j\hat{\mathbf{s}}_{Ei}^{1\,\mathrm{T}}\right)\end{aligned} \tag{26}$$

where $\mathrm{tr}(\cdot)$ is the trace of the matrix. To estimate $\mathbf{O}_{j1}$, we define the following:

$$\mathbf{Q} = \sum_{i=1}^{N}\hat{\mathbf{s}}_{Ei}^j\hat{\mathbf{s}}_{Ei}^{1\,\mathrm{T}} \tag{27}$$

where $\mathbf{Q}$ is a 3×3 matrix for the stable scattering centers and a 2×2 matrix for the sliding scattering centers. The SVD decomposition is applied on $\mathbf{Q}$, yielding the following:

$$\mathbf{Q} = \mathbf{U}\Sigma\mathbf{V}^{\mathrm{T}} \tag{28}$$

where $\mathbf{U}$ and $\mathbf{V}$ are the orthogonal matrices, Σ is a diagonal matrix composed of the singular values, and the diagonal elements are arranged in descending order. When there are more than two non-collinear stable scattering centers, or more than one non-collinear sliding scattering centers, $\mathbf{Q}$ is full rank. Then, the estimated transformation matrix $\mathbf{O}_{j1}$ is given by the following:

$$\hat{\mathbf{O}}_{j1} = \mathbf{U}\mathbf{V}^{\mathrm{T}} \tag{29}$$

For the proof of the algorithm, please refer to [28]. From (29), we find that $\hat{\mathbf{O}}_{j1}$ is the product of two orthogonal matrices; thus, it still is an orthogonal matrix, which satisfies the rotation matrix orthogonal constraint.

After obtaining the transformation matrix $\hat{\mathbf{O}}_{j1}$, we calculate the associated scattering center coordinates matrix and the radar LOS matrix, respectively, as follows:

$$\hat{\mathbf{S}}_R^j = \hat{\mathbf{O}}_{j1}\hat{\mathbf{S}}_E^j \tag{30}$$

$$\hat{\mathbf{C}}_R^j = \hat{\mathbf{O}}_{j1}\hat{\mathbf{C}}_E^j \tag{31}$$

Comparing (30) with (21), we find that the associated scattering centers coordinate reconstructed from the range sequences of the jth radar are consistent with the reference coordinates, and the multi-station data association is completed.

B. THE TARGET ABSOLUTE ATTITUDE ESTIMATION

After multi-station data association, the scattering center coordinates reconstructed from the other radars are consistent with those reconstructed from the reference radar. According to Section IV.A, a transformation matrix $\mathbf{O}_1$ exists between the associated scattering center coordinates and the absolute coordinates. In this section, we remove the effect of $\mathbf{O}_1$ and obtain the absolute coordinates of the scattering centers.

Fig. 4 shows the relationship between the reconstructed geometry and the absolute geometry at time t_k. The solid line is the target absolute scattering center coordinates and the

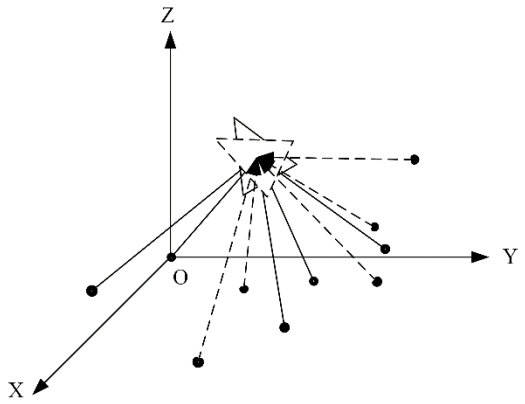

FIGURE 4. Relationship between the reconstructed geometry and the absolute geometry.

absolute radar LOSs, and the dotted line is the associated scattering center coordinates and radar LOSs at time t_k. A rotation matrix $\mathbf{O}_1^k$ exists between the associated scattering center coordinates matrix $\hat{\mathbf{S}}_R^1$ and the absolute scattering center coordinates matrix $\hat{\mathbf{S}}_k$ at time t_k; meanwhile, the same rotation matrix $\mathbf{O}_1^k$ exist between the associated radar LOS matrix $\hat{\mathbf{C}}_R^k$ at time t_k and the absolute radar LOS matrix $\hat{\mathbf{C}}_k$, where $\hat{\mathbf{C}}_R^k = \left[\hat{\mathbf{c}}_{R1}^k\ \hat{\mathbf{c}}_{R2}^k \cdots \hat{\mathbf{c}}_{RM}^k\right]$, in which $\hat{\mathbf{c}}_{Rj}^k$ is the kth column of $\hat{\mathbf{C}}_R^j$ and represents the associated LOS of the jth radar at time t_k. Therefore, we can estimate the transformation matrix $\mathbf{O}_1^k$ by the relationship between the associated radar LOSs and the absolute radar LOSs. Here, $\mathbf{O}_1^k$ is a 3×3 rotation matrix for the stable scattering centers and a 2×2 rotation matrix for the sliding scattering centers.

Assuming that the positions of the radars and the target centroid position are known, the absolute LOS unit vector of the jth radar at time t_k can be represented as the following:

$$\mathbf{c}_j^k = \frac{\mathbf{Z}_j - \mathbf{T}_k}{\left\|\mathbf{Z}_j - \mathbf{T}_k\right\|} \tag{32}$$

where $\mathbf{Z}_j$ is the position of the jth radar and $\mathbf{T}_k$ is the target centroid position at time t_k. The transformation error e between $\hat{\mathbf{C}}_R^k$ and $\hat{\mathbf{C}}_R^k$ is defined as follows:

$$e = \sum_{j=1}^{M} e_j^2 = \sum_{j=1}^{M} \left\|\mathbf{c}_j^k - \mathbf{O}_1^k \hat{\mathbf{c}}_{Rj}^k\right\|_2^2 \tag{33}$$

where e_j is the transformation error between the associated LOS and the absolute LOS of the jth radar at time t_k. Then the transformation matrix $\mathbf{O}_1^k$ estimation problem is to find a matrix that minimizes the transformation error e under the condition that the rotation matrix orthogonal constraint is met and can be expressed as follows:

$$\begin{aligned} &\min_{O_k} \sum_{j=1}^{M} \left\|\mathbf{c}_j^k - \mathbf{O}_1^k \hat{\mathbf{c}}_{Rj}^k\right\|^2 \\ &s.t.\ \mathbf{O}_1^k \mathbf{O}_1^{k\,\mathrm{T}} = \mathbf{O}_1^{k\mathrm{T}} \mathbf{O}_1^k = \mathbf{I} \end{aligned} \tag{34}$$

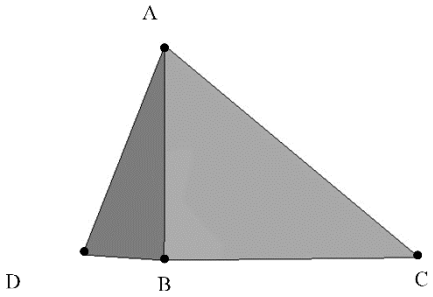

FIGURE 5. Target model composed of stable scattering centers.

where $\mathbf{I}$ is a 3×3 identity matrix for the stable scattering centers and a 2×2 identity matrix for the sliding scattering centers. The SVD method is applied again to solve the above optimization problem. When there are more than two non-coplanar $\mathbf{c}_j^k$ for the stable scattering centers reconstruction, or more than one non-coplanar $\mathbf{c}_j^k$ for the sliding scattering centers reconstruction, the algorithm has a unique solution. The estimated absolute scattering center coordinates at time t_k are given by the following:

$$\hat{\mathbf{S}}_k = \hat{\mathbf{O}}_1^k \hat{\mathbf{S}}_R^1 \tag{35}$$

where $\hat{\mathbf{S}}_R^1$ is the associated scattering center coordinates reconstructed from the range sequences of the reference radar and $\hat{\mathbf{S}}_R^1 = \hat{\mathbf{S}}_E^1$.

V. SIMULATION

In order to highlight the contributions of this paper, we perform three experiments to show the effectiveness of the proposed algorithm. The experiment environment and results are listed as follows:

A. THE RECONSTRUCTION OF THE STABLE SCATTERING CENTER COORDINATES

In this simulation, we verify the reconstruction performance of the proposed algorithm for the stable scattering centers. Fig. 5 is the target model composed of stable scattering centers. According to the electromagnetic scattering characteristics, the target contains 4 stable scattering centers distributed on the four vertices of the triangular pyramid, and the coordinates of the scattering centers in the object-fixed coordinate system are respectively [0, 0, 0.9m], [1m, 0, −0.6m], [0, 1.8m, −0.6m], and [−1.0392m, −0.6m, −0.6m]. The angular frequencies of spin and nutation are $w_s = \pi\, rad/s$, and $w_n = 2\pi\, rad/s$, respectively. The nutation angle is 10°, and the angle between the nutation axis and the Z axis of the reference coordinate system is 100°. The target is observed by three radars, and the bandwidth of the radars is 2 GHz, ranging from 8 GHz to 12 GHz. The azimuth and elevation angles of the radars in the object-fixed coordinate system are respectively [0°, 20°], [90°, 23°], and [−50°, 18°]. The radar pulse repetition frequency is 150 Hz and the data length is 2 s. Here we use CST software to generate the wideband echo data. First, the target model is generated in the

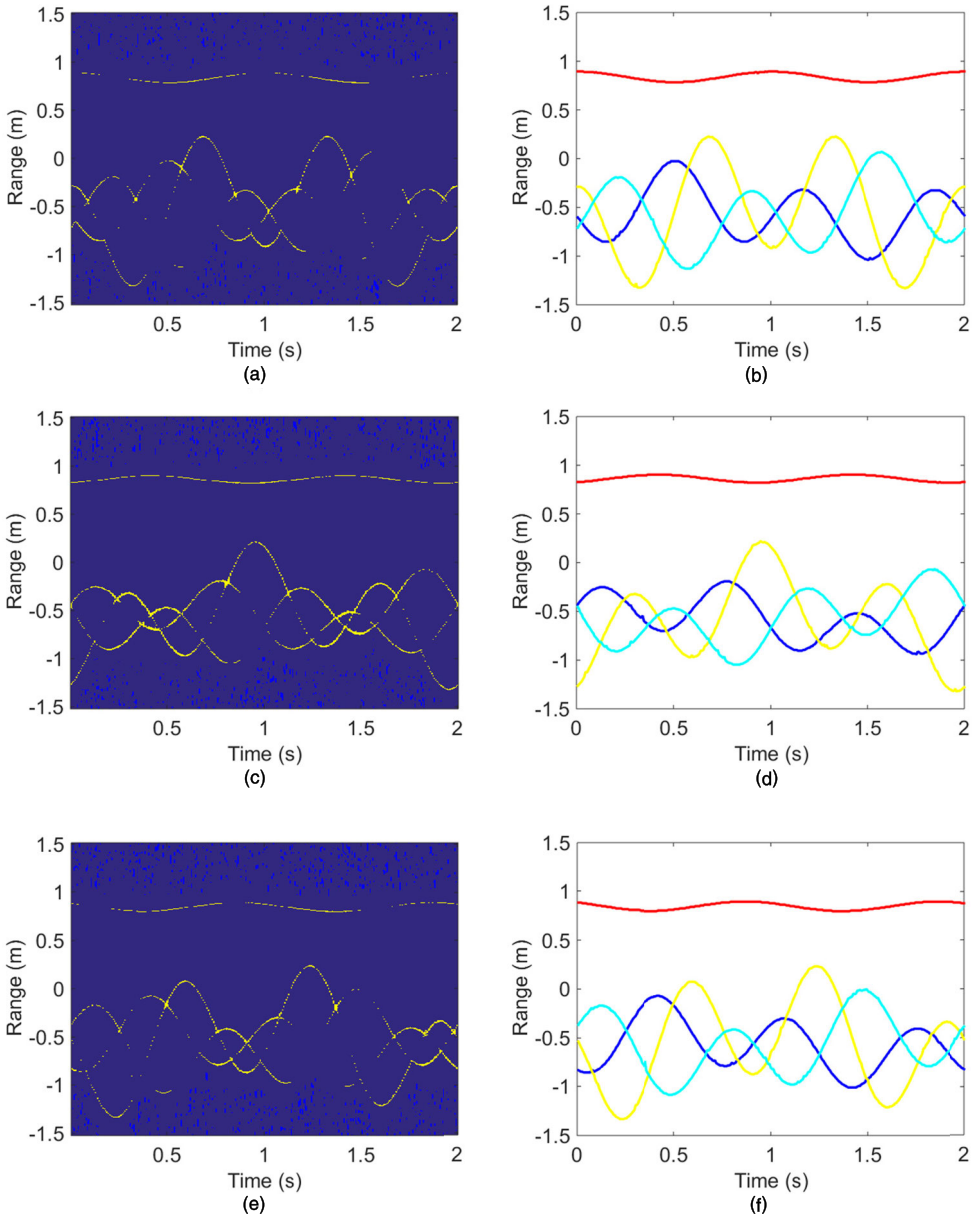

FIGURE 6. HRRP sequences and the extracted 1-D range sequences of the target. (a) HRRP sequences obtained from radar 1; (b) Extracted 1-D range sequences from radar 1; (c) HRRP sequences obtained from radar 2; (d) Extracted 1-D range sequences from radar 2; (e) HRRP sequences obtained from radar 3; (f) Extracted 1-D range sequences from radar 3.

CST based on the structural parameters of the target; then, the radar parameters and the azimuth and elevation angles of the radar LOSs calculated from the target motion parameters are input in the solver of the CST software, the wideband echoes of the target are obtained finally and used for 3-D scattering center coordinates reconstruction.

Fig. 6 shows the HRRP sequences and the extracted 1-D range sequences of the target. Fig. 6(a), (c) and (e) shows the target HRRP sequences obtained from three respective radar echoes obtained by the IAA algorithm. Each figure contains four curves, indicating that the target contains four scattering centers. Fig. 6(b), (d), and (f) shows the corresponding 1-D range sequences after range extraction and single-station association. In order to remove the glitch on the 1-D range curves caused by noise and wrong association, the Kalman smoothing algorithm is used to smooth the associate result a second time. Fig. 6 shows that the 1-D range sequences are consistent with the theoretical values.

Fig. 7 shows the 3-D scattering center coordinates reconstruction results. Fig. 7(a) shows the 3-D coordinates reconstruction results of four scattering centers at $t = 0.0067$s, and the specific coordinates of the scattering centers are listed in Table 1. Fig. 7(b) shows the 3-D motion trajectory of the scattering center B, and Fig. 7(c)-(e) shows projection of the scattering center motion on three coordinate axes. Fig. 7(a) and Table 1 indicate that the reconstructed scattering

TABLE 1. The absolute and reconstructed scattering center coordinates at $t = 0.0067$s.

	X (m)	Y (m)	Z (m)
A	0.8457	0	-0.3078
Reconstructed A	0.8523	0.0080	-0.3075
B	-0.5638	1	0.2052
Reconstructed B	-0.5890	1.0065	0.1904
C	-1.1795	0	-1.4862
Reconstructed C	-1.1870	-0.0514	-1.5083
D	-0.3586	-1.0392	0.7690
Reconstructed D	-0.3543	-1.0522	0.7846

center coordinates are consistent with the absolute coordinates. It can be seen from Fig. 7(c) that the 3-D motion of the scattering center B has a large reconstruction error at some time. This is because the 1-D range sequence of the scattering center B intersects with that of the scattering center C or D at these moments, and there will be an association error in the single-station association step.

The effect of signal-to-noise ratio (SNR) on the reconstruction performance of the proposed algorithm was studied and the results are below. We added the Gaussian white noise to the echo data generated by CST, the SNR ranged from 5 to 30 dB. Here, the echo SNR is defined as the ratio of the average energy of the single echo to the noise power. One hundred Monte Carlo experiments were performed on the target under each SNR, and the root normalized mean square error (RNMSE) of the reconstructed scattering center coordinates was used to measure the reconstruction performance. The RNMSE is defined as follows:

$$RNMSE = \sqrt{\frac{\sum_{k=1}^{K} \left\| \hat{S}_k^j - X_k^j \right\|_2^2}{\sum_{k=1}^{K} \left\| X_k^j \right\|_2^2}} \tag{36}$$

Fig. 8 shows the RNMSE of the reconstructed scattering centers coordinates versus SNR. From Fig. 8, we found that the reconstruction error of the proposed algorithm decreases as the SNR increases. The reconstruction error of the scattering center A is significantly smaller than that of the other three scattering centers. This is because the 1-D range sequence of the scattering center A has no intersection with the other range sequences, and the reconstruction error caused by the association error is avoided.

B. THE RECONSTRUCTION OF THE SLIDING SCATTERING CENTER COORDINATES

In this simulation, we verify the reconstruction performance of the proposed algorithm for the sliding scattering centers. Fig. 9 shows the target model composed of sliding scattering centers. According to the electromagnetic scattering characteristics, the target contains five scattering centers, where A is a stable scattering center and B–E are sliding scattering centers. The coordinates of the scattering centers A-E in the object-fixed coordinate system are respectively [0, 0.9m],

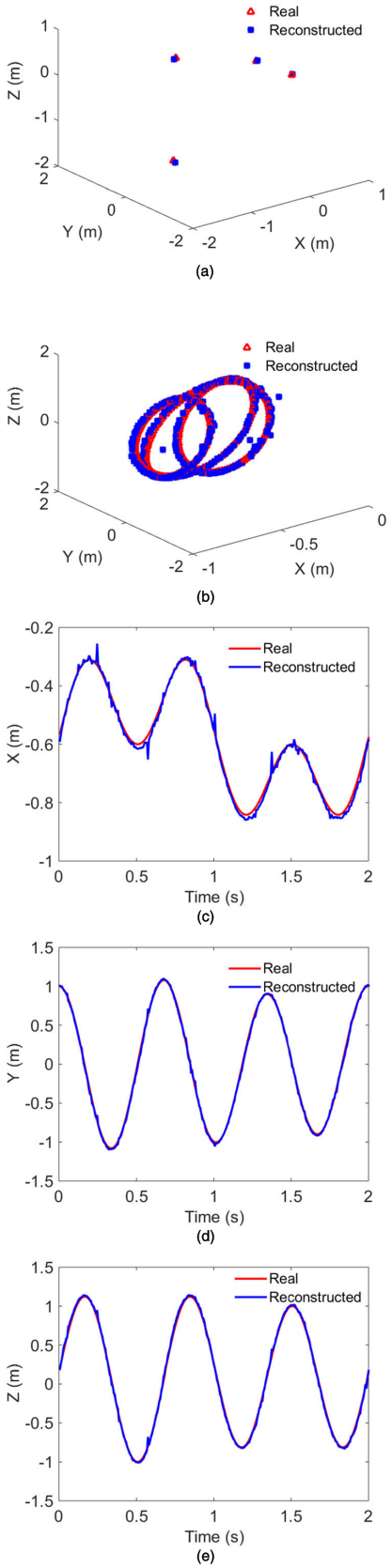

FIGURE 7. 3-D scattering center coordinates reconstruction results. (a) 3-D coordinates reconstruction results of four scattering centers at $t = 0.0067$ s; (b) 3-D motion trajectory of the scattering center B; (c) Projection of the scattering center B on X axis; (d) Projection of the scattering center B on Y axis; (e) Projection of the scattering center B on Z axis.

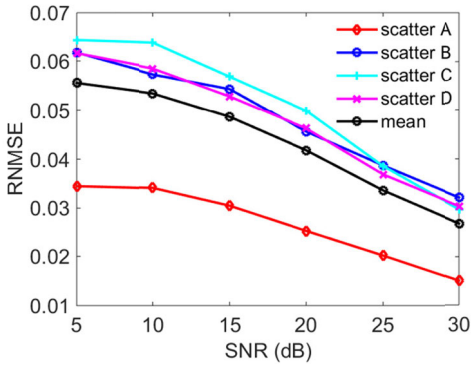

FIGURE 8. RNMSE of the reconstructed scattering centers coordinates versus SNR.

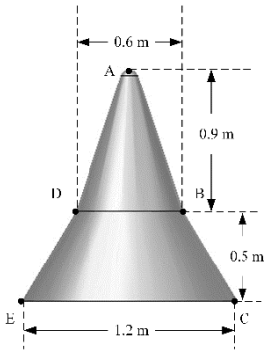

FIGURE 9. Target model composed of sliding scattering centers.

[0.3m, 0], [0.6m, −0.5m], [−0.3m, 0], and [−0.6m, −0.5m]. The angle frequency of spin and angular frequency of nutation are respectively $w_s = \pi\, rad/s$, and $w_n = 2\pi\, rad/s$. The nutation angle is 10°, and the angle between the nutation axis and the Z-axis of the reference coordinate system is 100°. The target is observed by two radars, The azimuth and pitch angle of the radar in the object-fixed coordinate system are 38° and 45° respectively. The other radar parameters are consistent with the parameters in Section V.A.

Fig. 10 shows the HRRP sequences and the extracted 1-D range sequences of the target. Fig. 10(a) and (c) shows the respective target HRRP sequences obtained from two radar echoes by the IAA algorithm. Fig. 10(b) and (d) are the corresponding 1-D range sequences after range extraction and single-station association. Three range curves can be observed in Fig. 10 because scatter D and E are sheltered and cannot be observed by the radars. The range sequences are consistent with the real values.

Fig. 11 shows the 2-D scattering center coordinates reconstruction result. Fig. 11(a) shows the results of the 2-D coordinates reconstruction of four scattering centers at $t = 0.0067$s, and the specific coordinates of the scattering centers are listed in Table 2. Fig. 11(b) shows the 2-D motion trajectory of the scattering center C, and Fig. 11(c) and (d) are the projection of the scattering center motion on two coordinate axes. Fig. 11(a) and Table 2

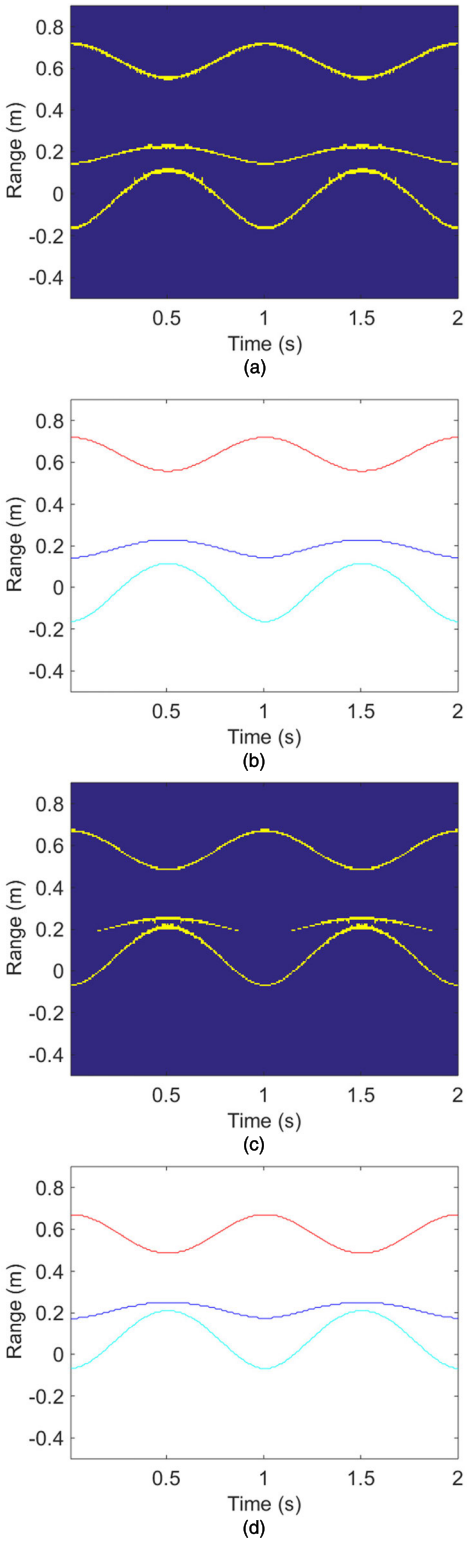

FIGURE 10. HRRP sequences and the extracted 1-D range sequences of the target. (a) HRRP sequences obtained from radar 1; (b) Extracted 1-D range sequences from radar 1; (c) HRRP sequences obtained from radar 2; (d) Extracted 1-D range sequences from radar 2.

indicate that the reconstructed scattering center coordinates are consistent with the absolute coordinates. In Fig. 11(d), the errors at the peaks and valleys are large. The large errors

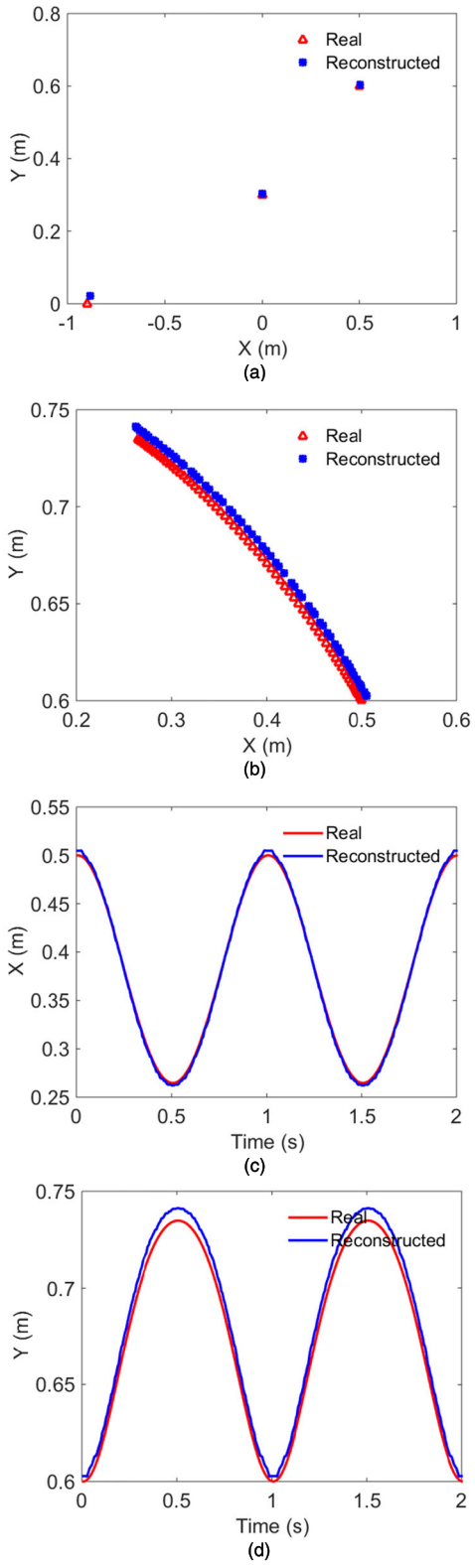

FIGURE 11. 2-D scattering center coordinates reconstruction result. (a) 3-D coordinates reconstruction results of four scattering centers at $t = 0.0067$ s; (b) 2-D motion trajectory of the scattering center C; (c) Projection of the scattering center C on X axis; (d) Projection of the scattering center C on Y axis.

are because the target projection range changes gradually at these locations; consequently, the error between the estimated range data and the real range is large, resulting in a large reconstruction error.

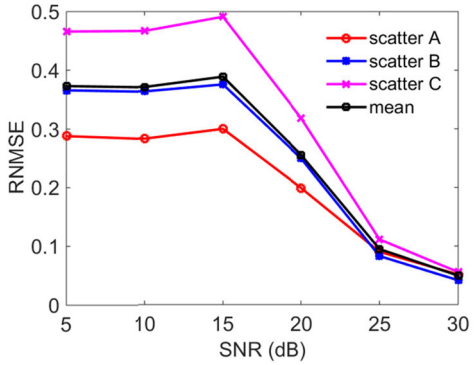

FIGURE 12. RNMSE of the reconstructed scattering centers versus SNR.

TABLE 2. The absolute and reconstructed scattering center coordinates at $t = 0.0067$s.

	X (m)	Z (m)
A	-0.9	0
Reconstructed A	-0.8838	0.0212
B	0	0.3
Reconstructed B	-0.0010	0.3032
C	0.5	0.6
Reconstructed C	0.5048	0.6028

In order to verify the anti-noise performance of the algorithm, Gaussian white noise was added to the echo signal generated by CST, and the echo SNR ranged from 5 to 30 dB. Then one hundred Monte Carlo experiments were performed under different SNR conditions. The variation of the RNMSE with the SNR is shown in Fig. 12. From Fig. 12, we can find that the reconstruction error of the algorithm decreases gradually before 25 dB and is stable after 25 dB. The reconstruction performance is worse than that in Section V.A, since the extracted range sequences are worse.

The above two experiments verify the effectiveness of the proposed algorithm, both for the target composed of stable scattering centers and for the target composed of sliding scattering centers.

C. THE COMPARISON EXPERIMENT WITH THE EXISTING ALGORITHM

In order to illustrate the superiority of the proposed algorithm in 3-D absolute attitude reconstruction, the 3-D reconstruction algorithm based on the target micro-motion model[17] is performed to rebuild the absolute coordinates of the scattering centers in the same condition of the experiment in Section V.A, except that the nutation angle is 10° plus a random perturbation. The SNR is set to be 30 dB. The reconstructed motion trajectories of the scattering center B by these two types of algorithms are shown in Fig. 13 (a) and (b), respectively. From Fig. 13, we can find that the reconstruction error of the reconstructed algorithm in [17] is greater than that of the proposed algorithm. This is because the transformation matrix estimation algorithm in [17] is an optimization algorithm based on the target micro-motion model. When

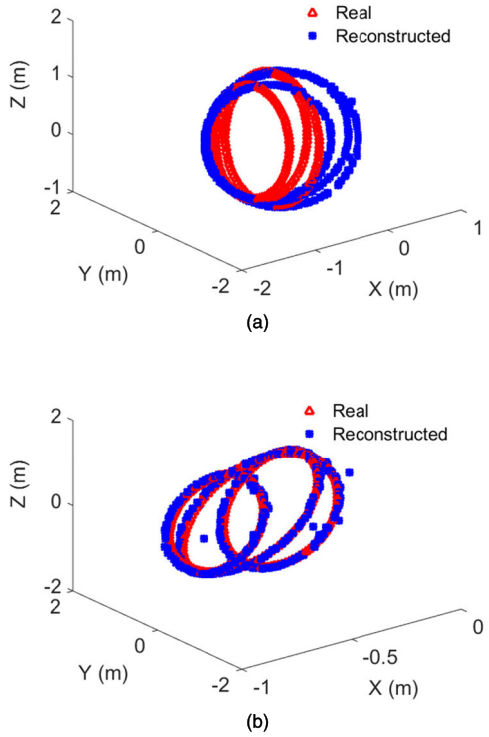

FIGURE 13. The comparison of the 3-D reconstruction algorithm in [17] and the proposed algorithm. (a) 3-D motion trajectory of the scattering center B reconstructed by the reconstruction algorithm in [17]; (b) 3-D motion trajectory of the scattering center B reconstructed by the proposed algorithm.

the assumed micro-motion model does not match the actual motion model, the transformation matrix obtained by the algorithm is inaccurate, so is the reconstructed absolute attitude of the scattering centers. By contrast, the transformation matrix is estimated from the multi-station data, so no target motion model knowledge is required. Thus, the 3-D absolute attitude reconstruction algorithm proposed in this paper can obtain more accurate results when dealing with real data due to the mismatch between the actual target motion and the micro-motion model.

VI. CONCLUSION

With the aim of resolving the warhead recognition problem, this study proposes a 3-D absolute attitude reconstruction algorithm based on multi-station HRRP sequences. This algorithm proposes the strategy of ''reconstruction before association''. In the reconstruction step, the single-station 1-D range data are extracted from the echo of each radar and are associated with the KF and the NNSF method. Then, the scattering center coordinates and radar LOS unit vectors are calculated from the 1-D range sequences by the factorization method. In the association step, the multi-station data are associated with the reconstructed scattering center coordinates, and the 3-D absolute attitude of the target is reconstructed by the relationship between the associated radar LOSs and the absolute radar LOSs. The 3-D reconstruction algorithm for the stable scattering centers and the sliding scattering centers are investigated. Simulation results show that the proposed algorithm can obtain good reconstruction effects, and the reconstructed 3-D absolute attitude are not affected by the mismatch of the micro-motion model. In practical application, the synchronization of multiple radars is a problem. Besides, the algorithm in this study only considers the continuous HRRP sequences. In actual observation, the HRRP sequences are usually incomplete due to certain reasons, including the occlusion effect and RCS fluctuation, and the discontinuous HRRP sequences should be considered in the subsequent work.

ACKNOWLEDGMENT

The authors would like to thank LetPub (www.letpub.com) for its linguistic assistance during the preparation of this manuscript.

REFERENCES

[1] V. Chen, F. Li, S.-S. Ho, and H. Wechsler, ''Micro-Doppler effect in radar: Phenomenon, model, and simulation study,'' *IEEE Trans. Aerosp. Electron. Syst.*, vol. 42, no. 1, pp. 2–21, Jan. 2006.

[2] P. Lei, J. Wang, and J. Sun, ''Analysis of radar micro-Doppler signatures from rigid targets in space based on inertial parameters,'' *IET Radar, Sonar Navigat.*, vol. 5, no. 2, p. 93, 2011.

[3] Y. Luo, Q. Zhang, C.-w. Qiu, X.-J. Liang, and K.-M. Li, ''Micro-Doppler effect analysis and feature extraction in ISAR imaging with stepped-frequency chirp signals,'' *IEEE Trans. Geosci. Remote Sens.*, vol. 48, no. 4, pp. 2087–2098, Apr. 2010.

[4] L. Hong, F. Dai, and X. Wang, ''Micro Doppler reconstruction from discontinuous observations based on gapped SBL-FBTVAR method for spin stabilized object,'' *IEEE Access*, vol. 7, pp. 104500–104513, 2019.

[5] X. Ai, Z. Xu, and F. Zhao, ''Feature extraction of micro-motional targets via time-range distribution,'' *IEEE Access*, vol. 7, pp. 118889–118897, 2019.

[6] X.-Y. Pan, J. Liu, L.-T. Xu, X. Ai, Q. Xie, B. Yu, and C. Li, ''Extraction of micro-Doppler frequency from HRRPs of rotating targets,'' *IEEE Access*, vol. 5, pp. 26162–26174, 2017.

[7] T. Wang, X. Wang, Y. Chang, J. Liu, and S. Xiao, ''Estimation of precession parameters and generation of ISAR images of ballistic missile targets,'' *IEEE Trans. Aerosp. Electron. Syst.*, vol. 46, no. 4, pp. 1983–1995, Oct. 2010.

[8] J. Sun, S. Shang, and J. D. Xu, ''3-D shape reconstruction from range measurements of ISAR,'' in *Proc. Int. Conf. Wavelet Active Media Technol. Inf. Process. (ICWAMTIP)*, Chengdu, China, 2012, pp. 25–28. [Online]. Available: http://ieeexplore.ieee.org/stamp/stamp.jsp?tp=&arnumber=6413431&isnumber=6413424

[9] G. Wang, X.-G. Xia, and V. Chen, ''Three-dimensional ISAR imaging of maneuvering targets using three receivers,'' *IEEE Trans. Image Process.*, vol. 10, no. 3, pp. 436–447, Mar. 2001.

[10] J. Given and W. Schmidt, ''Generalized ISAR—Part II: Interferometric techniques for three-dimensional location of scatterers,'' *IEEE Trans. Image Process.*, vol. 14, no. 11, pp. 1792–1797, Nov. 2005.

[11] X. Xu and R. Narayanan, ''Three-dimensional interferometric ISAR imaging for target scattering diagnosis and modeling,'' *IEEE Trans. Image Process.*, vol. 10, no. 7, pp. 1094–1102, Jul. 2001.

[12] L. Liu, F. Zhou, X.-R. Bai, M.-L. Tao, and Z.-J. Zhang, ''Joint cross-range scaling and 3d geometry reconstruction of ISAR targets based on factorization method,'' *IEEE Trans. Image Process.*, vol. 25, no. 4, pp. 1740–1750, Apr. 2016.

[13] M. A. Stuff, P. Sanchez, and M. Biancalana, ''Extraction of threedimensional motion and geometric invariants from range dependent signals,'' *Multidimensional Syst. Signal Process.*, vol. 14, pp. 161–181, Jan. 2003.

[14] M. Ferrara, G. Arnold, and M. Stuff, ''Shape and motion reconstruction from 3d-to-1d orthographically projected data via object-image relations,'' *IEEE Trans. Pattern Anal. Mach. Intell.*, vol. 31, no. 10, pp. 1906–1912, Oct. 2009.

[15] J. Zhou, H. Zhou, and Q. Fu, "A novel method for reconstructing 3D scattering centers based on multiple HRR profiles and its performance bounds," in *Proc. CIE Int. Conf. Radar*, 2006, pp. 1–4. [Online]. Available: http://ieeexplore.ieee.org/stamp/stamp.jsp?tp=&arnumber=4148167&isnumber=4118064
[16] W. Jun, Y. Dong, Z. Yuxi, and W. Shaoming, "3-D imaging algorithm for targets with micro-motion based on HRRP sequence," in *Proc. 2nd Int. Conf. Signal Process. Syst.*, 2010, p. V2-283. [Online]. Available: http://ieeexplore.ieee.org/stamp/stamp.jsp?tp=&arnumber=5555491&isnumber=5555203
[17] L. Hong, F. Dai, and H. Liu, "Motion-parameter estimation for precession-with-nutation space targets based on wideband radar measurements," *IEEE Trans. Aerosp. Electron. Syst.*, vol. 52, no. 2, pp. 643–657, Apr. 2016.
[18] Y. Bi, S. Wei, J. Wang, and S. Mao, "3D imaging of rapidly spinning space targets based on a factorization method," *Sensors*, vol. 17, no. 2, pp. 366–384, Feb. 2017.
[19] S. Wu and L. Hong, "Modelling 3D rigid-body object motion and structure estimation with HRR/GMTI measurements," *IET Control Theory Appl.*, vol. 1, no. 4, pp. 1023–1032, Jul. 2007.
[20] K. Suwa, T. Wakayama, and M. Iwamoto, "Estimation of target motion and 3D target geometry using multistatic ISAR movies," in *Proc. IEEE Int. Geosci. Remote Sens. Symp.*, Jul. 2009, p. V-429. [Online]. Available: http://ieeexplore.ieee.org/stamp/stamp.jsp?tp=&arnumber=5417640&isnumber=5417612
[21] G. Li, J. Zou, S. Xu, B. Tian, and Z. Chen, "A method of 3D reconstruction via ISAR Sequences based on scattering centers association for space rigid object," *Proc. SPIE*, vol. 9252, Oct. 2014, Art. no. 92520N. [Online]. Available: https://spie.org/Publications/Proceedings/Paper/10.1117/12.2067006?SSO=1
[22] G. Di, F. Su, H. Yang, and S. Fu, "ISAR image scattering center association based on speeded-up robust features," *Multimedia Tools Appl.*, pp. 1–18, Jun. 2018. [Online]. Available: https://link.springer.com/article/10.1007/s11042-018-6291-z
[23] Y. Zhou, L. Zhang, Y. Cao, and Z. Wu, "Attitude estimation and geometry reconstruction of satellite targets based on ISAR image sequence interpretation," *IEEE Trans. Aerosp. Electron. Syst.*, vol. 55, no. 4, pp. 1698–1711, Aug. 2019.
[24] Q.-Y. Qu, K.-Y. Guo, and X.-Q. Sheng, "An accurate bistatic scattering center model for extended cone-shaped targets," *IEEE Trans. Antennas Propag.*, vol. 62, no. 10, pp. 5209–5218, Oct. 2014.
[25] M. Spirito, "On the accuracy of cellular mobile station location estimation," *IEEE Trans. Veh. Technol.*, vol. 50, no. 3, pp. 674–685, May 2001.
[26] T. Yardibi, J. Li, P. Stoica, M. Xue, and A. B. Baggeroer, "Source localization and sensing: A nonparametric iterative adaptive approach based on weighted least squares," *IEEE Trans. Aerosp. Electron. Syst.*, vol. 46, no. 1, pp. 425–443, Jan. 2010.
[27] S. Changyu, D. Lan, H. Xun, and L. Hongwei, "Multiple target tracking based separation of Micro-Doppler signals from coning target," in *Proc. IEEE Radar Conf.*, May 2014, pp. 0130–0133. [Online]. Available: http://ieeexplore.ieee.org/stamp/stamp.jsp?tp=&arnumber=6875570&isnumber=6875503
[28] K. S. Arun, T. S. Huang, and S. D. Blostein, "Least-squares fitting of two 3-D point sets," *IEEE Trans. Pattern Anal. Mach. Intell.*, vol. PAMI-9, no. 5, pp. 698–700, Sep. 1987.
[29] T. E. Abrudan, J. Eriksson, and V. Koivunen, "Steepest descent algorithms for optimization under unitary matrix constraint," *IEEE Trans. Signal Process.*, vol. 56, no. 3, pp. 1134–1147, Mar. 2008.
[30] Z. Jianxiong, Z. Hongzhong, S. Zhiguang, and F. Qiang, "Global scattering center model extraction of radar targets based on wideband measurements," *IEEE Trans. Antennas Propag.*, vol. 56, no. 7, pp. 2051–2060, Jul. 2008.

NAN SU received the B.S. degree in electronic engineering from Xidian University, Xi'an, China, in 2012, where he is currently pursuing the Ph.D. degree in signal processing with the National Laboratory of Radar Signal Processing. His research interests include micro-motion feature extraction and parameter estimation.

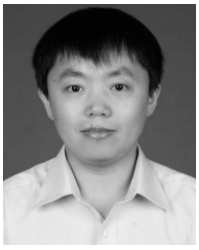

FENGZHOU DAI received the B.S., M.S., and Ph.D. degrees in electronic engineering from Xidian University, Xi'an, China, in 2002, 2005, and 2010, respectively. He is currently an Associate Professor with the National Laboratory of Radar Signal Processing, Xidian University. His research interests include radar signal processing and microwave imaging.

HONGWEI LIU received the B.S. degree from the Dalian University of Technology, Dalian, China, in 1992, and the M.S. and Ph.D. degrees from Xidian University, Xi'an, China, in 1995 and 1999, respectively. He is currently a Professor and the Director of the National Laboratory of Radar Signal Processing, Xidian University. His research interests include radar automatic target recognition, netted radar, radar signal processing and detection, and adaptive signal processing.

BO ZHANG received the B.S. degrees in electronic engineering from Xidian University, Xi'an, China, in 2014, where he is currently pursuing the Ph.D. degree in signal processing with the National Laboratory of Radar Signal Processing. His research interests include MIMO radar waveform design and radar target detection.